# Superconducting Filaments Formed During Nonvolatile Resistance Switching in Electrodeposited $\delta$-$Bi_2O_3$

**Jakub A. Koza, Eric W. Bohannan, and Jay A. Switzer***

Department of Chemistry and Graduate Center for Materials Research, Missouri University of Science and Technology, Rolla, Missouri 65409-1170, United States

**ABSTRACT** We show that electrodeposited films of $\delta$-$Bi_2O_3$ in a Pt/$\delta$-$Bi_2O_3$/Au cell exhibit unipolar resistance switching. After being formed at a large electric field of 40 MV/m, the cell can be reversibly switched between a low resistance state (156 Ω) and a high resistance state (1.2 GΩ) by simply cycling between SET and RESET voltages of the same polarity. Because the high and low resistance states are persistent, the cell is a candidate for nonvolatile resistance random access memory (RRAM). A Bi nanofilament forms at the SET voltage, and it ruptures to form a 50 nm gap during the RESET step at a current density of $2 \times 10^7$ A/cm$^2$. The diameter of the Bi filament is a function of the compliance current, and can be tuned from 140 to 260 nm, but the current density in the RESET step is independent of the Bi diameter. An electromigration rupture mechanism is proposed. The Bi nanofilaments in the low resistance state are superconducting, with a $T_c$ of 5.8 K and an $H_c$ of 5 kOe. This is an unexpected result, because bulk Bi is not a superconductor.

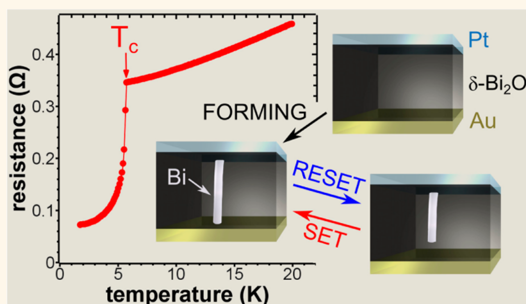


**KEYWORDS:** electrodeposition · nonvolatile resistance switching · solid-state memory · superconductive filaments · $Bi_2O_3$ · bismuth

An emerging solid-state, nonvolatile memory known as resistance random access memory (RRAM) can be produced when a metal oxide that undergoes resistance switching is sandwiched between two metallic electrodes.[1−6] Because the resistance of the metal oxide is a function of the history of charge that has passed through the material, RRAM devices have been described as memristors.[7−9] Compared with current nonvolatile memory based on charge storage, RRAM is expected to allow the use of smaller memory cells.[1,3,4] Metal oxides that undergo resistance switching include $TiO_2$,[8,10] $TaO_x$,[11,12] $Fe_2O_3$,[13] NiO,[13−18] ZnO,[19−21] CoO,[13,18] $Co_3O_4$,[22,23] $Cu_2O$,[24,25] CuO,[26,27] $Fe_3O_4$,[28] $CoFe_2O_4$,[29] $VO_2$,[30] and $(Bi_2O_3)_{0.7}(Y_2O_3)_{0.3}$.[31] Although the mechanism of resistance switching in the metal oxides is not well understood, the transport of oxygen vacancies or oxide ions is generally considered to be important.[10,32] $\delta$-$Bi_2O_3$ is a particularly interesting material for this application, because it has the highest known oxide ion mobility and it has very high electrical resistivity. $\delta$-$Bi_2O_3$ is the high-temperature cubic polymorph of $Bi_2O_3$. It is only thermodynamically stable at temperatures above 729 °C, but it can be stabilized in the face-centered-cubic structure at room temperature by forming a solid solution with cubic oxides such as $Y_2O_3$. Shi *et al.* have demonstrated that $(Bi_2O_3)_{0.7}(Y_2O_3)_{0.3}$ films sandwiched between Ag and Pt electrodes exhibit electric field induced resistance switching.[31] We previously reported that additive-free $\delta$-$Bi_2O_3$ can be electrodeposited at 65 °C from aqueous solution.[33,34] Here, we show that electrodeposited films of $\delta$-$Bi_2O_3$ in a Pt/$\delta$-$Bi_2O_3$/Au cell exhibit unipolar resistance switching, and we demonstrate that superconducting nanofilaments of Bi metal are produced during the switching process. Although Zhu *et al.* have reported superconductivity in a Nb/ZnO/Pt bipolar resistance switching cell, the superconductivity was attributed to nanofilaments of Nb metal, a known superconductor.[35] The observation of superconductivity in our Pt/$\delta$-$Bi_2O_3$/Au cells, however, is an unexpected result, because bulk Bi is not a superconductor. It only occurs when the Bi nanofilaments are formed. Besides the possibility of using the material

* Address correspondence to jswitzer@mst.edu.

Received for review July 23, 2013 and accepted September 30, 2013.

**Published online** September 30, 2013
10.1021/nn4038207

© 2013 American Chemical Society

for solid-state memory, the electrodeposited $\delta$-$Bi_2O_3$ may find future utility in applications in which it is necessary to toggle between an insulating material with GΩ-cm resistivity and a superconductor by a simple flip of a switch.

## RESULTS AND DISCUSSION

Films of $\delta$-$Bi_2O_3$ were electrodeposited onto Au substrates to a thickness of 1.3 $\mu$m.[34] The films deposit with a strong [111] orientation and a columnar microstructure (see Figure S1, Supporting Information). The resistivity of the as-deposited $\delta$-$Bi_2O_3$ is typically $6.5 \times 10^9$ Ω cm. A top Pt contact to the film was made by sputtering a 200 nm thick circular pad of Pt with a 125 $\mu$m diameter through a shadow mask. As shown in Figure 1, the electrodeposited $\delta$-$Bi_2O_3$ films exhibit unipolar resistance switching. That is, the Pt/$\delta$-$Bi_2O_3$/Au cell can be switched from a high resistance state (HRS) to a low resistance state (LRS) without changing the voltage polarity. The sample is first "formed" by increasing the applied bias to approximately 60 V (see inset of Figure 1a). This FORMING bias corresponds to a very large electric field of about 40 MV/m. A compliance current of 50 $\mu$A was used in both the FORMING and SET steps in order to prevent irreversible, hard dielectric breakdown. A conducting filament is produced during the FORMING process, and the initial resistance of about $10^{10}$ Ω abruptly drops to about 150 Ω. After the FORMING step, the cell can be switched from the LRS to the HRS by a RESET process, and then switched from the HRS to the LRS by a SET process. The conducting filament is produced during the FORMING and SET steps at high electric fields, and it is ruptured during the RESET step at high current densities. A cartoon showing the generation of the conducting filament during the FORMING and SET steps and rupture of the filament during the RESET step is shown in Figure 1b. The rupture of the filament near the negative electrode is consistent with an electromigration rupture mechanism, as discussed later in this paper. In the RESET step a compliance current is not applied and the current reaches a value of $4.4 \pm 2.5$ mA, far above the value of the compliance current of 50 $\mu$A applied in the SET step. In the RESET step the filament is ruptured at the RESET voltage ($0.4 \pm 0.1$ V) and the cell switches to the HRS.

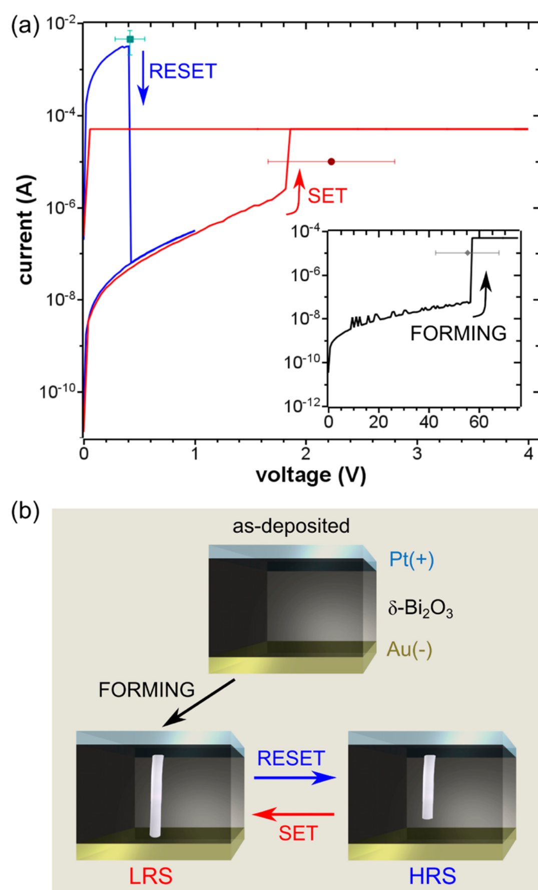


**Figure 1. Unipolar resistance switching in the Pt/$\delta$-$Bi_2O_3$/Au cell. (a) Current–voltage curves for the Pt/$\delta$-$Bi_2O_3$/Au cell during the FORMING, SET, and RESET steps. Solid points represent average switching parameters measured on 10 different contacts together with their standard deviations. The voltage was scanned at a rate of 0.7 V/s. (b) Schematic showing the formation of a conducting filament during the FORMING and SET steps, and rupture of the filament during the RESET step.**

The cell can be switched back to its LRS by performing the SET process. The SET process is similar in nature to the FORMING step. However, because only the gap in the ruptured filament has to be reformed, it occurs at much lower voltage ($2.2 \pm 0.6$ V) than in the FORMING step. The solid points in Figure 1a represent average switching parameters with their standard deviations collected from 10 different contacts. The switching parameters scatter significantly in the initial switching cycles following the FORMING step. Therefore, the analysis is performed after the parameters stabilize, usually after about 25 switching cycles. There is at least a 1 V difference between the RESET and SET voltages in each switching cycle, which minimizes the risk of a hard dielectric breakdown in the cell when switching the cell to HRS. The cell can be switched between the LRS and HRS multiple times (Figure 2a), and the states are persistent (Figure 2b). One issue that needs to be addressed is the maximum number of switches the material can perform. Although the 100 cycles shown in the endurance test in Figure 2a are encouraging, practical devices will require thousands or millions of switching cycles. The ratio of resistance between the HRS and LRS of $10^6$ (Figure 2a,b) would allow one to easily distinguish between the two states of the cell in a real working device.

The electrical properties of the Pt/$\delta$-$Bi_2O_3$/Au cell in each of its states were measured by impedance spectroscopy. Figure 3 shows the impedance spectra in Nyquist (complex) coordinates, together with the equivalent circuits used for fitting the three states.

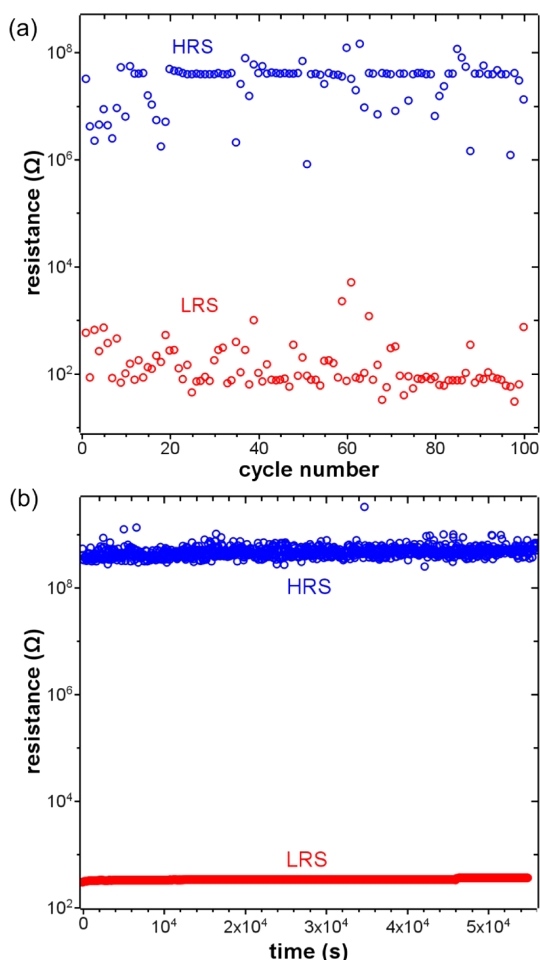


Figure 2. (a) Endurance test of the Pt/$\delta$-$Bi_2O_3$/Au cell showing 100 cycles. (b) Stability of the high resistance state (HRS) and low resistance state (LRS) over time. FORMING and SET steps performed with 50 $\mu$A compliance current.

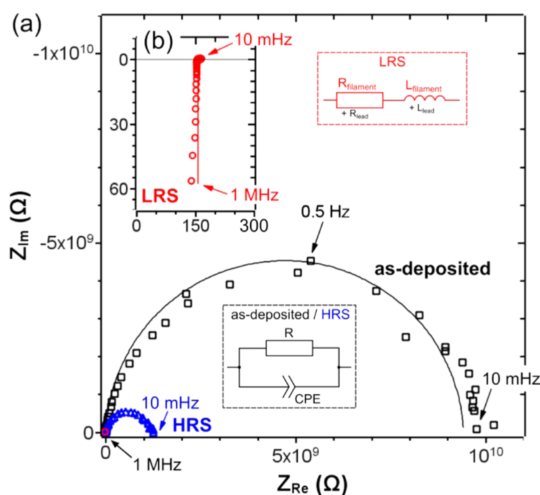


Figure 3. Impedance spectra of the Pt/$\delta$-$Bi_2O_3$/Au resistance switching cell in (a) as-deposited state (black), high resistance state (HRS, blue), and (b) low resistance state (LRS, red). Points are experimental results and lines are fits to the equivalent circuits, which are shown as insets. A constant phase element (CPE) is used to model the capacitor. FORMING and SET steps performed with 50 $\mu$A compliance current.

The cell in the as-deposited state can be described by a single time constant, because a single semicircle is observed (black squares in Figure 3). Assuming a constant phase element (CPE), the as-deposited state has a small capacitance of only 23 pF, with a parallel resistance of 9.4 GΩ, corresponding to a resistivity for $\delta$-$Bi_2O_3$ of 6.5 × $10^9$ Ωcm. The LRS shows resistive behavior (Figure 3b) with a small series inductance, which originates from the cables. The resistive behavior is suggestive of a metallic nature for the filaments. The resistance of the LRS is only 156 Ω, compared with the initial 9.4 GΩ of the as-deposited film. After the RESET step, the cell is in the HRS. As with the as-deposited state, the HRS can be described by a capacitance with a parallel resistance (blue triangles in Figure 3). The capacitance of the HRS state is 25 pF, and the resistance is 1.2 GΩ. The lower resistance of the HRS compared with the as-deposited state is consistent with a gap in the filament that is smaller than the original film thickness. The measured capacitance of the HRS is slightly larger than that of the as-deposited film. Because the filament is in parallel with the rest of the film, the measured 25 pF of the HRS is the sum of the small capacitance from the broken filament and the larger capacitance contributed by the electrode area.

The impedance spectra for the Pt/$\delta$-$Bi_2O_3$/Au cell are similar to those observed by other researchers for Pt/NiO/Pt and Au/CuO/Pt resistance switching cells.[14,26] In the NiO and CuO cells it was suggested that the filaments were metallic. In the case of the NiO-based cell, the formation of Ni filaments at the NiO grain boundaries was confirmed by TEM.[15] Metallic filament formation in the Pt/NiO/Pt cell was also confirmed by magnetic measurements.[17] The filaments were shown to be ferromagnetic, with a clear exchange coupling between the ferromagnetic Ni filaments and the antiferromagnetic NiO matrix.[17]

The metallic nature of the conducting filaments was confirmed by the temperature dependence of the resistance for the LRS (Figure 4). The measurements also showed that the conducting filaments were superconducting at low temperature. These measurements were made using pressed In contacts to the top surface instead of the Pt contacts used in the switching experiments. The pressed In contacts always produce a LRS state that has a lower resistance than the Pt contacts. The cells produced with the In contacts can be reversibly switched between the HRS and the LRS. Figure S2 in the Supporting Information shows *R vs T* curves for films with a variety of pressed In contacts, and Figure S3 shows FORMING, RESET, and SET curves for a cell using pressed In contacts. As shown in the inset of Figure 4a, the resistance of the LRS decreases linearly as the temperature is decreased from 300 to 5.8 K. This linear dependence is consistent with the filaments being metallic Bi. At 5.8 K there is an abrupt

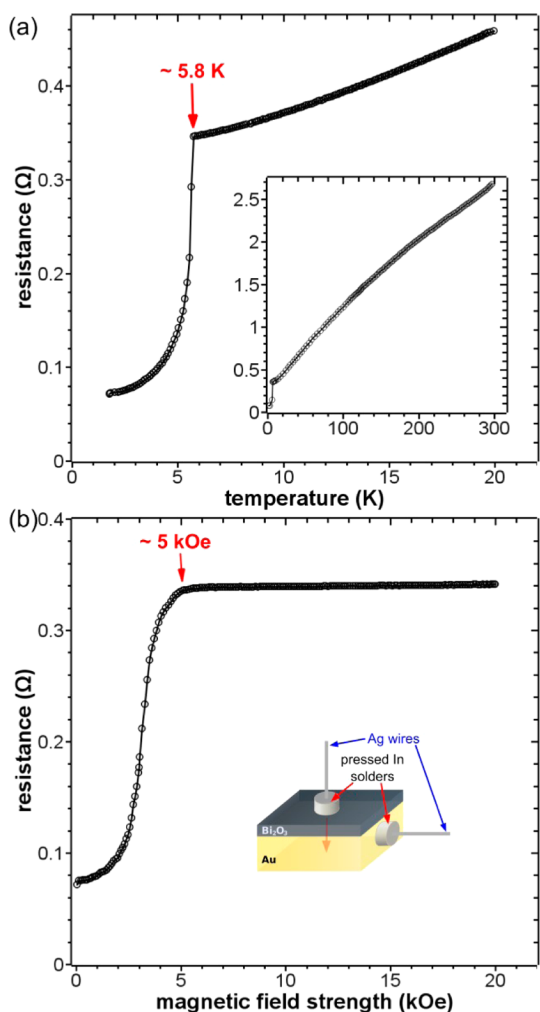


**Figure 4. Evidence for superconductivity in the conducting filaments. (a) Resistance *vs* temperature dependence at 0 Oe of the $\delta$-$Bi_2O_3$-based cell in the low resistance state, SET with a compliance current of 100 $\mu$A. The inset shows the *R*(*T*) dependence from 300 K at 0 Oe. (b) Resistance *vs* magnetic field strength dependence measured at 1.8 K. The inset in (b) shows the measurement geometry used in the experiments.**

drop in the resistance, the signature of a superconductor material. As shown in Figure 4b, the superconductivity is quenched at about 5 kOe for a sample that was held at 1.8 K. This large critical field is consistent with type II superconductivity. The measured $T_c$ and $H_c$ are higher than those observed for In metal ($T_c^{In}$ = 3.4 K, $\mu_0 H_c^{In}$ = 28.15 mT)[36] that was used for our top contact. We have also observed superconductivity in samples using an Au top contact (see Figure S4, Supporting Information). Although bulk Bi is not a superconductor, it has been shown by other workers that Bi nanowires electrodeposited into polycarbonate membranes also exhibit type II superconductivity.[37,38] The electrodeposited Bi nanowires had two distinct superconducting phases with $T_c$ of 7.2 and 8.3 K, and corresponding $H_c$ of 10 and 45 kOe. The superconductivity was explained by the formation of high-pressure Bi phases at the grain boundaries.[37] It has also been observed,

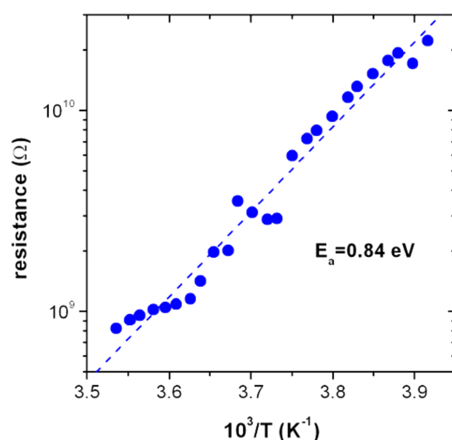


**Figure 5. Plot of log(resistance) *vs* reciprocal temperature for the $\delta$-$Bi_2O_3$-based cell in the high resistance state. The activation energy of 0.84 eV is consistent with $\delta$-$Bi_2O_3$ being in the gap that forms after the RESET step (low resistance state SET at a compliance current of 100 $\mu$A).**

however, that single-crystal Bi nanowires are superconducting,[39] and that electrodeposited Bi nanowires that were removed from membranes had a $T_c$ of 1.3 K and an $H_c$ of 40 kOe.[38] In the latter case, the superconductivity was attributed to the formation of a thin oxide film at the wire surface.[38] This would be similar to the conducting filaments in the LRS of our Pt/$\delta$-$Bi_2O_3$/Au resistance switching cell, because the Bi filaments would be surrounded by the $\delta$-$Bi_2O_3$ matrix. Because the $\delta$-$Bi_2O_3$ deposits with a [111] orientation and a columnar microstructure,[34] the conducting filaments likely form along columnar grain boundaries, as proposed for a strongly textured, columnar ZnO-based cell.[19] The metallic behavior in the *R vs T* curve and the observation of a superconducting signature in Figure 4 are strong evidence that the conducting filaments in the LRS are metallic Bi. Without direct observation of the filaments, we cannot completely rule out the possibility that the conducting filaments are due to nonstoichiometric bismuth oxide that is produced during the FORMING and SET processes. However, we would expect such a cell to exhibit bipolar rather than unipolar resistance switching.

After the Pt/$\delta$-$Bi_2O_3$/Au cell is RESET, the HRS is produced due to the rupture of the Bi filament. The temperature dependence of the resistivity of the HRS was studied to gain insight into the nature of the material in the gap that forms when the Bi filament ruptures. The cell switches to insulating behavior, because the resistance increases exponentially as the temperature is lowered. An Arrhenius plot is shown for the HRS in Figure 5. The activation energy measured from this plot is 0.84 eV, in reasonable agreement with the known activation energy of 0.99 eV for $\delta$-$Bi_2O_3$.[40] This Arrhenius measurement suggests that the gap is filled either with $\delta$-$Bi_2O_3$, or with a material with similar electrical properties.

The diameter of the Bi filaments that are produced in the SET step can be controlled by the compliance

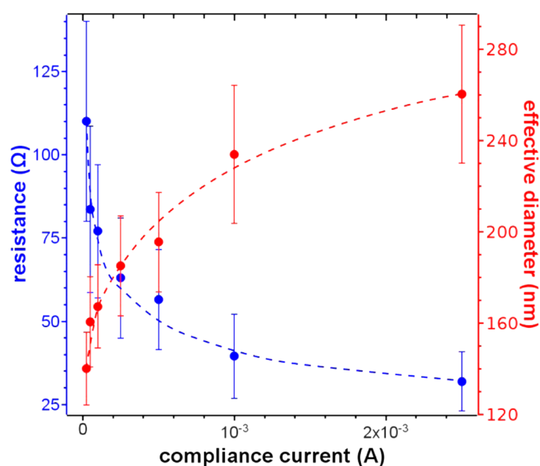


**Figure 6. Filament resistance (blue, left axis) and effective diameter (red, right axis) *vs* compliance current of the Pt/δ-$Bi_2O_3$/Au cell in the low resistance state. The diameter of the filament increases as the compliance current is increased. The dashed lines are drawn as a guide to an eye. Cell was switched at a scan rate of 0.7 V/s.**

current that is used during the SET process. Although we have not directly observed the Bi filaments by microcopy, we estimated their effective diameter from the measured resistance of the low resistance state. The filaments were SET and RESET at least 25 times prior to the analysis to ensure stable switching parameters. We used the measured resistance and known film thickness (1.3 $\mu$m), and we assumed that the Bi filaments are cylindrical in shape and have the same resistivity ($128 \times 10^{-8}$ Ωm) as bulk Bi.[41] As shown in Figure 6, the filament resistance decreases and the effective Bi filament diameter increases as the compliance current is increased. A decrease in filament resistance with increasing compliance current was also reported for Pt/$Co_3O_4$/Pt and Cu/$TiO_x$/$TaO_x$/W resistance switching cells.[22,42] In the latter case the filaments were metallic Cu and the filament diameter was estimated using the same method as outlined in this paper for the Pt/δ-$Bi_2O_3$/Au cell. The Bi filament diameter increases from 140 ± 16 nm at a compliance current of 25 $\mu$A to 260 ± 30 nm at a compliance current of 2.5 mA.

The systematic increase in the effective diameter with increasing compliance current also causes an increase in the RESET current that is necessary to rupture the filaments (see Figure 7). Although the voltage required to SET and RESET the Pt/δ-$Bi_2O_3$/Au cell is independent of the compliance current, the RESET current increases as the compliance current and Bi diameter are increased. These results show that it is the applied *electric field* that reduces δ-$Bi_2O_3$ to Bi filaments in the FORMING and SET steps, and it is the applied *current* that ruptures the Bi filaments during the RESET steps. Although the RESET current and Bi diameter are both dependent on the compliance current, the current density for filament rupture during

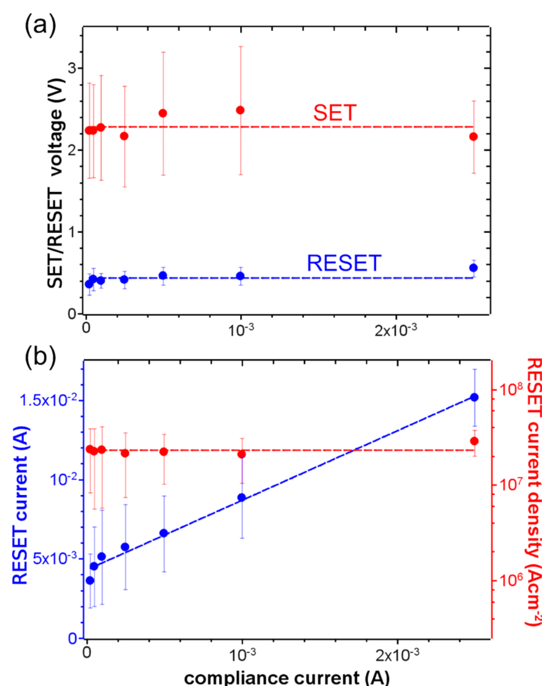


**Figure 7. (a) SET (red) and RESET (blue) voltages *vs* compliance current used in the SET step for the Pt/δ-$Bi_2O_3$/Au cell. (b) Dependence of the RESET current (left, blue) and the RESET current density (right, red) on the compliance current used in the SET step. The RESET current increases as the compliance current increases, but the RESET current density is independent of compliance current. Points represent average values measured on 10 different contacts together with their standard deviations. Cell was switched at a scan rate of 0.7 V/s.**

the RESET step is fairly constant at $2.2 \pm 0.2 \times 10^7$ A/cm$^2$ (see Figure 7b).

It is also possible to estimate the gap size after the Bi filament ruptures. Here, we compare the voltage (60 V) required to FORM the entire 1.3 $\mu$m film thickness with that (2.2 V) required to SET the cell. If we assume that the gap is filled with a material of similar breakdown field strength as the as-deposited δ-$Bi_2O_3$ (40 MV/m), the gap size is estimated to be approximately 50 nm. Because the SET voltage is not a function of the compliance current used to form and RESET the cell, the gap size appears to be independent of the compliance current.

The mechanism of film rupture is presently not known. On the basis of the estimated diameters of the Bi filaments, the average current density in the RESET step is $2.2 \pm 0.2 \times 10^7$ A/cm$^2$. The RESET current density is independent of the effective diameter of the Bi nanofilaments. The large current density in the RESET step would lead to Joule heating of the filament to induce either thermal oxidation of the Bi filaments or even melting of the filaments. Another possible mechanism for the rupture of the filament is current-induced electromigration, in which metal atoms move in the direction of electron flow due to momentum transfer. This electromigration would lead to a gap formation at the negative

electrode, with thickening of the filament toward the positive electrode. The cartoon shown in Figure 1b is consistent with the electromigration-induced film rupture. Electromigration is a common problem in large-scale integration, in which interconnects rupture due to high current flow.[43] The current densities observed in the RESET step of our Pt/$\delta$-$Bi_2O_3$/Au are greater than or equal to those that produce electromigration in interconnects.

## CONCLUSIONS

We have shown that the Pt/$\delta$-$Bi_2O_3$/Au cell undergoes unipolar resistance switching. Because the low and high resistance states that are formed are persistent, this cell is a candidate for future RRAM devices. The voltage difference between the LRS and HRS is over 1 V, and the resistance contrast between the two states is over $10^6$. Our results are consistent with the formation and rupture of a conducting filament of Bi metal. The effective diameter of the Bi filaments is in the 140−260 nm range and can be controlled by varying the compliance current used to SET the cell. The gap that is formed after resetting the cell is estimated to be 50 nm in length, and is independent of the compliance current. The Bi nanowires in the low resistance state are superconducting, with a $T_c$ of 5.8 K, and an $H_c$ of 5 kOe. A very large applied electric field of 40 MV/m reduces $\delta$-$Bi_2O_3$ to Bi filaments in the FORMING step, and a large applied current density of 2.2 $\pm$ 0.2 $\times$ $10^7$ A/cm$^2$ ruptures the Bi filaments during the RESET step. The current density necessary to effect filament rupture is independent of the filament diameter. Joule heating and/or current-driven electromigration are possible mechanisms for the rupture of the Bi nanofilaments. Because the electrodeposition method we use to deposit the $\delta$-$Bi_2O_3$ is not a line-of-sight deposition method like sputtering and the material only deposits on electrified interfaces, it should be possible in future work to deposit the material conformally onto crossbar arrays to produce highly scalable memory.

## MATERIALS AND METHODS

$\delta$-$Bi_2O_3$ films were electrodeposited to a thickness of 1.3 $\mu$m according to the procedure described elsewhere.[33,34] Briefly, films were anodically deposited at a current density of 5 mA/cm$^2$ and a temperature of 65 °C onto Au substrates. The electrolyte used consisted of 0.1 M $Bi(NO_3)_3$, 0.25 M L-tartaric acid and 2.5 M KOH. The substrates were mechanically polished and then electropolished prior to the electrodeposition of the $\delta$-$Bi_2O_3$ films.[33] The structure of the films was determined using a high-resolution Philips X-Pert MRD X-ray diffractometer (XRD) with a Cu K$\alpha_1$ radiation source ($\lambda$ = 1.54056 Å). The morphology of films was studied by scanning electron microscopy (SEM; Hitachi S4700 FESEM).

Resistance switching experiments were performed in two-point, vertical geometry using a Keithley 2400 current source. A top Pt contact to the film was made by sputtering a 200 nm thick circular pad of Pt with a 125 $\mu$m diameter through a shadow mask. The connection to the Pt pad was made with a sharp Au low-pressure pin contact. An electrical connection was made to the Au substrate using Cu tape, which served as the bottom contact. Current−voltage curves were run at a scan rate of 0.7 V/s, with the top Pt contact as the positive electrode.

The electrical properties of the Pt/$\delta$-$Bi_2O_3$/Au cell in each of its states were measured by impedance spectroscopy using a Solartron SI 1255 frequency response analyzer in the frequency range of 1 MHz to 10 mHz. The as-deposited material, HRS, and LRS were measured with AC amplitudes of 1 V, 50 mV, and 10 mV, respectively.

Electrical and magnetotransport measurements were performed in the Quantum Design Physical Property Measurement System (PPMS). Two Ag wires were attached to the film and to the Au substrate by pressing In solder, which served as electrical contacts. The resistance was measured with a two-point method normal to the film plane. The LRS was measured at 25 $\mu$A, while the HRS was measured at 1 nA.

*Conflict of Interest:* The authors declare no competing financial interest.

*Acknowledgment.* This material is based upon work supported by the U.S. Department of Energy, Office of Basic Energy Sciences, Division of Materials Sciences and Engineering, under Grant No. DE-FG02-08ER46518 (superconducting transition measurements), and the National Science Foundation under Grants DMR-1104801 and ECCS-1310425 (film deposition, resistance switching measurements).

*Supporting Information Available:* SEM micrograph of electrodeposited $\delta$-$Bi_2O_3$ showing columnar microstructure, *R vs T* curves for films with a variety of pressed In top contacts, FORMING, SET, and RESET curves for films using pressed In contacts, and observation of superconductivity in a device using a low-pressure Au pin contact. This material is available free of charge *via* the Internet at http://pubs.acs.org.

## REFERENCES AND NOTES


1. Yang, J. J.; Inoue, I. H.; Mikolajick, T.; Hwang, C. S. Metal Oxide Memories Based on Thermochemical and Valence Change Mechanisms. *MRS Bull.* **2012**, *37*, 131–137.
2. Waser, R.; Dittmann, R.; Staikov, G.; Szot, K. Redox-Based Resistive Switching Memories—Nanoionic Mechanisms, Prospects, and Challenges. *Adv. Mater.* **2009**, *21*, 2632–2663.
3. Strukov, D. B.; Kohlstedt, H. Resistive Switching Phenomena in Thin Films: Materials, Devices, and Applications. *MRS Bull.* **2012**, *37*, 108–114.
4. Sawa, A. Resistive Switching in Transition Metal Oxides. *Mater. Today* **2008**, *11*, 28–36.
5. Lee, M. H.; Hwang, C. S. Resistive Switching Memory: Observations with Scanning Probe Microscopy. *Nanoscale* **2011**, *3*, 490–502.
6. Doo Seok, J.; Reji, T.; Katiyar, R. S.; Scott, J. F.; Kohlstedt, H.; Petraru, A.; Cheol Seong, H. Emerging Memories: Resistive Switching Mechanisms and Current Status. *Rep. Prog. Phys.* **2012**, *75*, 076502.
7. Chua, L. O. Memristor—The Missing Circuit Element. *IEEE Trans. Circuit Theory* **1971**, *18*, 507–519.
8. Strukov, D. B.; Snider, G. S.; Stewart, D. R.; Williams, R. S. The Missing Memristor Found. *Nature* **2008**, *453*, 80–83.
9. Chua, L. Resistance Switching Memories are Memristors. *Appl. Phys. A: Mater. Sci. Process.* **2011**, *102*, 765–783.
10. Yang, J. J.; Pickett, M. D.; Li, X.; Ohlberg, D. A. A.; Stewart, D. R.; Williams, R. S. Memristive Switching Mechanism for Metal/Oxide/Metal Nanodevices. *Nat. Nanotechnol.* **2008**, *3*, 429–433.
11. Lee, M.-J.; Lee, C. B.; Lee, D.; Lee, S. R.; Chang, M.; Hur, J. H.; Kim, Y.-B.; Kim, C.-J.; Seo, D. H.; Seo, S.; *et al.* A Fast, High-Endurance and Scalable Non-Volatile Memory Device Made from Asymmetric $Ta_2O_5/TaO_2$ Bilayer Structures. *Nat. Mater.* **2011**, *10*, 625–630.

12. Antonio, C. T.; John Paul, S.; Gilberto, M.-R.; Williams, R. S. Sub-Nanosecond Switching of a Tantalum Oxide Memristor. *Nanotechnology* **2011**, *22*, 485203.
13. Inoue, I. H.; Yasuda, S.; Akinaga, H.; Takagi, H. Nonpolar Resistance Switching of Metal/Binary-Transition-Metal Oxides/Metal Sandwiches: Homogeneous/Inhomogeneous Transition of Current Distribution. *Phys. Rev. B: Condens. Matter Mater. Phys.* **2008**, *77*, 035105.
14. You, Y.-H.; So, B.-S.; Hwang, J.-H.; Cho, W.; Lee, S. S.; Chung, T.-M.; Kim, C. G.; An, K.-S. Impedance Spectroscopy Characterization of Resistance Switching NiO Thin Films Prepared through Atomic Layer Deposition. *Appl. Phys. Lett.* **2006**, *89*, 222105.
15. Lee, M.-J.; Han, S.; Jeon, S. H.; Park, B. H.; Kang, B. S.; Ahn, S.-E.; Kim, K. H.; Lee, C. B.; Kim, C. J.; Yoo, I.-K.; *et al.* Electrical Manipulation of Nanofilaments in Transition-Metal Oxides for Resistance-Based Memory. *Nano Lett.* **2009**, *9*, 1476–1481.
16. Lee, M.-J.; Kim, S. I.; Lee, C. B.; Yin, H.; Ahn, S.-E.; Kang, B. S.; Kim, K. H.; Park, J. C.; Kim, C. J.; Song, I.; *et al.* Low-Temperature-Grown Transition Metal Oxide Based Storage Materials and Oxide Transistors for High-Density Non-Volatile Memory. *Adv. Funct. Mater.* **2009**, *19*, 1587–1593.
17. Son, J. Y.; Kim, C. H.; Cho, J. H.; Shin, Y.-H.; Jang, H. M. Self-Formed Exchange Bias of Switchable Conducting Filaments in NiO Resistive Random Access Memory Capacitors. *ACS Nano* **2010**, *4*, 3288–3292.
18. Shima, H.; Takano, F.; Akinaga, H.; Tamai, Y.; Inoue, I. H.; Takagi, H. Resistance Switching in the Metal Deficient-Type Oxides: NiO and CoO. *Appl. Phys. Lett.* **2007**, *91*, 012901.
19. Zi-Jheng, L.; Jen-Chun, C.; Shih-Yuan, W.; Jin-Yiew, G.; Tri-Rung, Y. Improved Resistive Switching of Textured ZnO Thin Films Grown on Ru Electrodes. *IEEE Electron Device Lett.* **2011**, *32*, 1728–1730.
20. Yang, Y.; Zhang, X.; Gao, M.; Zeng, F.; Zhou, W.; Xie, S.; Pan, F. Nonvolatile Resistive Switching in Single Crystalline ZnO Nanowires. *Nanoscale* **2011**, *3*, 1917–1921.
21. Qi, J.; Olmedo, M.; Ren, J.; Zhan, N.; Zhao, J.; Zheng, J.-G.; Liu, J. Resistive Switching in Single Epitaxial ZnO Nano-islands. *ACS Nano* **2012**, *6*, 1051–1058.
22. Nagashima, K.; Yanagida, T.; Oka, K.; Taniguchi, M.; Kawai, T.; Kim, J.-S.; Park, B. H. Resistive Switching Multistate Nonvolatile Memory Effects in a Single Cobalt Oxide Nanowire. *Nano Lett.* **2010**, *10*, 1359–1363.
23. Gao, X.; Guo, H.; Xia, Y.; Yin, J.; Liu, Z. Unipolar Resistive Switching Characteristics in $Co_3O_4$ Films. *Thin Solid Films* **2010**, *519*, 450–452.
24. Chen, A.; Haddad, S.; Wu, Y. C.; Lan, Z.; Fang, T. N.; Kaza, S. Switching Characteristics of $Cu_2O$ Metal-Insulator-Metal Resistive Memory. *Appl. Phys. Lett.* **2007**, *91*, 123517.
25. Kang, S.-O.; Hong, S.; Choi, J.; Kim, J.-S.; Hwang, I.; Byun, I.-S.; Yun, K.-S.; Park, B. H. Electrochemical Growth and Resistive Switching of Flat-Surfaced and (111)-Oriented $Cu_2O$ Films. *Appl. Phys. Lett.* **2009**, *95*, 092108.
26. Kim, C. H.; Jang, Y. H.; Hwang, H. J.; Sun, Z. H.; Moon, H. B.; Cho, J. H. Observation of Bistable Resistance Memory Switching in CuO Thin Films. *Appl. Phys. Lett.* **2009**, *94*, 102107.
27. Yasuhara, R.; Fujiwara, K.; Horiba, K.; Kumigashira, H.; Kotsugi, M.; Oshima, M.; Takagi, H. Inhomogeneous Chemical States in Resistance-Switching Devices with a Planar-Type Pt/CuO/Pt Structure. *Appl. Phys. Lett.* **2009**, *95*, 012110.
28. Switzer, J. A.; Gudavarthy, R. V.; Kulp, E. A.; Mu, G.; He, Z.; Wessel, A. J. Resistance Switching in Electrodeposited Magnetite Superlattices. *J. Am. Chem. Soc.* **2010**, *132*, 1258–1260.
29. He, Z.; Koza, J. A.; Mu, G.; Miller, A. S.; Bohannan, E. W.; Switzer, J. A. Electrodeposition of $Co_xFe_{3-x}O_4$ Epitaxial Films and Superlattices. *Chem. Mater.* **2012**, *25*, 223–232.
30. Koza, J. A.; He, Z.; Miller, A. S.; Switzer, J. A. Resistance Switching in Electrodeposited $VO_2$ Thin Films. *Chem. Mater.* **2011**, *23*, 4105–4108.
31. Shi, L.; Shang, D. S.; Sun, J. R.; Shen, B. G. Electric Field-Induced Resistance Switching in $(Bi_2O_3)_{0.7}(Y_2O_3)_{0.3}$ Films. *J. Appl. Phys.* **2009**, *105*, 083714.
32. Lee, H. D.; Magyari-Köpe, B.; Nishi, Y. Model of Metallic Filament Formation and Rupture in NiO for Unipolar Switching. *Phys. Rev. B: Condens. Matter Mater. Phys.* **2010**, *81*, 193202.
33. Switzer, J. A.; Shumsky, M. G.; Bohannan, E. W. Electrodeposited Ceramic Single Crystals. *Science* **1999**, *284*, 293–296.
34. Bohannan, E. W.; Jaynes, C. C.; Shumsky, M. G.; Barton, J. K.; Switzer, J. A. Low-Temperature Electrodeposition of the High-Temperature Cubic Polymorph of Bismuth(III) Oxide. *Solid State Ionics* **2000**, *131*, 97–107.
35. Zhu, X.; Su, W.; Liu, Y.; Hu, B.; Pan, L.; Lu, W.; Zhang, J.; Li, R.-W. Observation of Conductance Quantization in Oxide-Based Resistive Switching Memory. *Adv. Mater.* **2012**, *24*, 3941–3946.
36. *Springer Handbook of Condensed Matter and Materials Data*; Martienssen, W., Warlimont, H., Eds.; Springer: Berlin, 2005.
37. Tian, M.; Wang, J.; Kumar, N.; Han, T.; Kobayashi, Y.; Liu, Y.; Mallouk, T. E.; Chan, M. H. W. Observation of Superconductivity in Granular Bi Nanowires Fabricated by Electrodeposition. *Nano Lett.* **2006**, *6*, 2773–2780.
38. Tian, M.; Wang, J.; Zhang, Q.; Kumar, N.; Mallouk, T. E.; Chan, M. H. W. Superconductivity and Quantum Oscillations in Crystalline Bi Nanowire. *Nano Lett.* **2009**, *9*, 3196–3202.
39. Zuxin, Y.; Hong, Z.; Haidong, L.; Wenhao, W.; Zhiping, L. Observation of Superconductivity in Single Crystalline Bi Nanowires. *Nanotechnology* **2008**, *19*, 085709.
40. Agasiev, A. A.; Zeinally, A. K.; Alekperov, S. J.; Guseinov, Y. Y. Photoelectrical Properties of $\delta$-$Bi_2O_3$ Thin Films. *Mater. Res. Bull.* **1986**, *21*, 765–771.
41. Focke, A. B.; Hill, J. R. The Electrical Resistivity of Bismuth Single Crystals. *Phys. Rev.* **1936**, *50*, 179–184.
42. Rahaman, S. Z.; Maikap, S.; Tien, T.-Ch.; Lee, H.-Y.; Chen, W.-S.; Chen, F. T.; Kao, M.-J.; Tsai, M.-J. Excellent Resistive Memory Characteristics and Switching Mechanism Using Ti Nanolayer at the Cu/$TaO_x$ Interface. *Nanoscale Res. Lett.* **2012**, *7*, 345–11.
43. Tu, K. N. Recent Advances on Electromigration in Very-Large-Scale-Integration of Interconnects. *J. Appl. Phys.* **2003**, *94*, 5451–5473.